Article

Current Biology

Effects of Sexual Experience and Puberty on Mouse Genital Cortex revealed by Chronic Imaging

Graphical Abstract

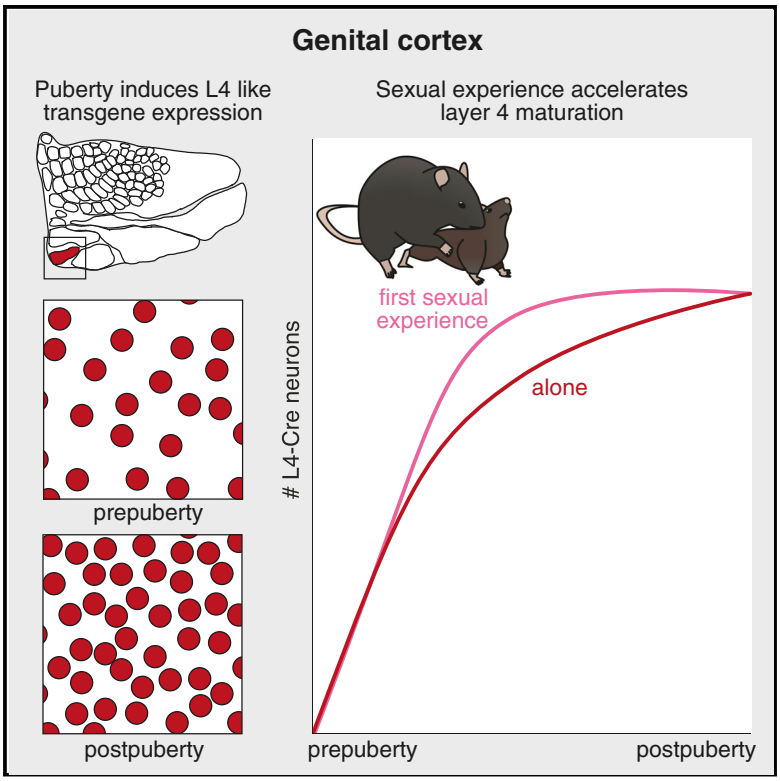

Authors

Johanna Sigl-Glöckner, Eduard Maier, Naoya Takahashi, Robert Sachdev, Matthew Larkum, Michael Brecht

Correspondence

michael.brecht@bccn-berlin.de

In Brief

Sigl-Glöckner et al. perform cell-type-specific imaging of genital cortex. They find that in genital cortex, the number of neurons with layer-4-like transgene expression increases during puberty, which could be rapidly advanced by sexual experience. Ca^{2+} imaging also revealed stronger responses in genital cortex of males compared to females.

Highlights

- Puberty induces layer-4-like transgene expression in genital cortex
- Such changes are absent in hindpaw cortex
- Sexual experience rapidly advances the increase of layer-4-like neurons
- Ca^{2+} imaging reveals stronger responses in male genital cortex compared to females

Sigl-Glöckner et al., 2019, Current Biology *29*, 3588–3599
November 4, 2019
https://doi.org/10.1016/j.cub.2019.08.062

CellPress

CellPress

Current Biology
Article

Effects of Sexual Experience and Puberty on Mouse Genital Cortex revealed by Chronic Imaging

Johanna Sigl-Glöckner,[1] Eduard Maier,[1] Naoya Takahashi,[2] Robert Sachdev,[2] Matthew Larkum,[2] and Michael Brecht[1,3,*]
[1]Bernstein Center for Computational Neuroscience Berlin, Humboldt-Universität zu Berlin, Philippstr. 13, Haus 6, 10115 Berlin, Germany
[2]Institute for Biology, Humboldt-Universität zu Berlin, Charitéplatz 1, 10437 Berlin, Germany
[3]Lead Contact
*Correspondence: michael.brecht@bccn-berlin.de
https://doi.org/10.1016/j.cub.2019.08.062

SUMMARY

The topographic map in layer 4 of somatosensory cortex is usually specified early postnatally and stable thereafter. Genital cortex, however, undergoes a sex-hormone- and sexual-touch-dependent pubertal expansion. Here, we image pubertal development of genital cortex in Scnn1a-Tg3-Cre mice, where transgene expression has been shown to be restricted to layer 4 neurons with primary sensory cortex identity. Interestingly, during puberty, the number of Scnn1a+ neurons roughly doubled within genital cortex. The increase of Scnn1a+ neurons was gradual and rapidly advanced by initial sexual experience. Neurons that gained Scnn1a expression comprised stellate and pyramidal neurons in layer 4. Unlike during neonatal development, pyramids did not retract their apical dendrites during puberty. Calcium imaging revealed stronger genital-touch responses in Scnn1a+ neurons in males versus females and a developmental increase in responsiveness in females. The first sexual interaction is a unique physical experience that often creates long-lasting memories. We suggest such experience uniquely alters somatosensory body maps.

INTRODUCTION

For many years, it has been recognized that the precise topographic representation of the body surface by the cortical input layer 4 is determined by peripheral inputs [1]. Based on findings from the barrel cortex, a consensus emerged that this topographic map of the body is established within the first postnatal week [2, 3] and shows little plasticity later in life [4]. However, there appears to be one exception to this rule of early and experience-independent map specification in layer 4 of somatosensory cortex: the region of rat somatosensory cortex that responds to genital stimulation, genital cortex, undergoes an unusually late expansion during puberty [5–7]. Furthermore, much like the onset of puberty [8], this expansion was dependent on sexual maturation and could be advanced by co-housing prepubertal female rats with adult males [6]. This plasticity of genital cortex is remarkable in several respects: (1) it occurs at a late postnatal stage; (2) the extent of remodeling is large; (3) it can be induced by physiological stimuli, whereas macroscopically detectable cortical plasticity usually requires drastic interference with incoming sensory signals, such as amputation or nerve transection [9]; and (4) it can be detected anatomically, unlike other somatosensory plasticity phenomena, which can only be revealed physiologically [4]. The expansion has been quantified by measuring the area receiving thalamic afferents within this somatosensory field [6].

The observation that, during puberty, thalamic fibers invade surrounding dysgranular regions of layer 4 [6] is particularly interesting because of the intricate relationship between thalamocortical axons and postsynaptic cortical neurons. In 1782, Francesco Gennari described the thick band of highly myelinated thalamic axons terminating in layer 4 [10]. After discovering fundamental differences in the physiology of primary and secondary (or higher order) cortical areas [11], their neurogenetic underpinnings have become evident more recently. Within somatosensory cortex, areal specification depends on various molecular cues and input from the ventral posteromedial nucleus of the thalamus [12–14]. Postsynaptically, thalamocortical axons target excitatory pyramidal and spiny stellate cells, the latter being a hallmark of primary somatosensory cortex [15–17]. Within layer 4, all excitatory neurons appear pyramidal-like at birth [18]. By postnatal day 5, however, the majority of neurons have a spiny stellate shape, suggesting that pyramidal neurons retract their apical dendrite to become stellates within the first postnatal week [18, 19]. Without thalamocortical input, stellate cells fail to develop appropriately [12, 14, 20].

We have previously shown that rat genital cortex grows during puberty, which we revealed by visualizing antibody-stained thalamocortical afferents within layer 4 [6]. Therefore, we wonder whether there are concurrent, cell-type-specific changes within layer 4. To address this question, we now turn to mice, where we can combine chronic two-photon imaging with the genetically targeted expression of fluorescent indicators. Specifically, we use the layer-4-specific transgenic mouse line Scnn1a-Tg3-Cre mice, where cre-recombinase expression resembles the homunculus in primary somatosensory cortex while septa are lacking Scnn1a+ neurons [21, 22]. Moreover, Scnn1a+ neurons exhibit the transcriptional profile of primary somatosensory layer 4 neurons [19]. Scnn1a+ neurons express the RAR-related orphan receptor beta (RORβ), a layer 4 marker [12, 23], whose ectopic expression is necessary and sufficient to orchestrate the acquisition of morphological, physiological, and circuit properties of primary layer 4 neurons [19]. Using this mouse line, we

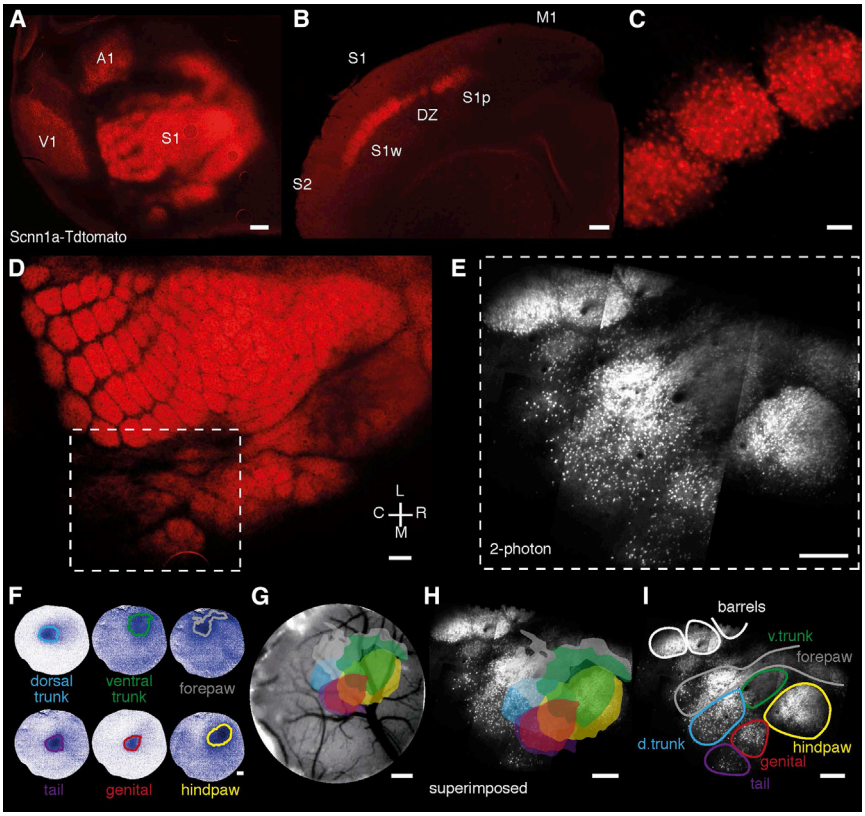

Figure 1. Mapping Scnn1a Expression and Genital Cortex in Scnn1a-tdTomato Mice

(A) Scnn1a-tdTomato tangential section. Scnn1a expression is dense in primary somatosensory (S1), auditory (A1), and visual (V1) cortex. Scale bar represents 500 μm.

(B) Scnn1a-tdTomato coronal section. Scnn1a expression is high in L4 whisker (S1w) and paw barrels (S1p) but low in the dysgranular zone (DZ), primary motor cortex (M1), secondary somatosensory cortex (S2), and non-layer 4 cells. Scale bar represents 250 μm.

(C) Within L4, Scnn1a+ neurons are confined to barrels and are absent from septa between barrels. Scale bar represents 50 μm.

(D) Scnn1a-tdTomato tangential section. Scnn1a expression reveals the S1 homunculus (male; P25). Scale bar represents 250 μm.

(E) The region of S1 highlighted by the dashed box in (D) imaged using two-photon microscopy. Multiple z stacks were acquired at minimal magnification (1,065 × 1,065 μm) and tiled together. Scale bar represents 250 μm.

(F) Intrinsic imaging (male; P25) revealed S1 subfields (dark blue) on the surface of the craniotomy representing the dorsal and ventral trunk, forepaw, tail, genital, and hindpaw. Scale bar represents 250 μm.

(G) Regions circled in (F) were aligned to each other based on the blood vessel pattern on the surface of the craniotomy. Scale bar represents 250 μm.

(H) Superimposing intrinsically mapped body parts (F and G) onto the expression of Scnn1a+ neurons in L4 of S1 as shown in (E) based on the blood vessel pattern. The topographic arrangement of subfields revealed by intrinsic imaging aligns with Scnn1a+ dense areas in L4 is shown. Scale bar represents 250 μm.

(I) Based on the alignment in (H), we infer that the barrel-like subfields of Scnn1a+ neurons within L4 represent the mapped body parts as shown. Scale bar represent 250 μm.

See also Figure S1.

investigate the following questions: first, does Scnn1a expression, which resembles the mouse homunculus, change in genital cortex during puberty? If so, what are the dynamics of this process? Second, do excitatory neurons in genital cortex remodel during puberty? Third, does puberty modulate the activity of genital cortex neurons? And finally, are there experience-dependent effects on pubertal maturation of layer 4 in genital cortex? More specifically, we want to find out whether initial sexual experience, usually conceptualized as particularly dramatic and memorable, modulates genital cortex maturation [24, 25].

RESULTS

Functional Identification of Genital Cortex in Scnn1a-tdTomato Mice

To investigate the cellular development of layer 4 (L4) in genital cortex, we used L4-specific Scnn1a-Tg3-cre mice [21], which we crossed with an Ai9 reporter line to label all cre-expressing neurons with td-Tomato. Tangential histological slices through cortical L4 of such Scnn1a-tdTomato brains reveal transgene expression limited to primary sensory cortices (Figure 1A; female; postnatal day [P] 40), with the homunculus being clearly visible within primary somatosensory cortex (S1). Coronal sections (Figure 1B) showed that Scnn1a expression is restricted to L4, where it is high in whisker (S1w) and paw (S1p) barrels, low in the dysgranular zone (DZ) and secondary somatosensory cortex (S2), and absent from motor cortex (M1) [26]. Furthermore, Scnn1a+ neurons are confined to barrels, and septa do not contain Scnn1a+ neurons (Figure 1C). We conclude that Scnn1a+ is a marker for primary sensory L4 neurons located in zones of dense lemniscal innervation [19, 22].

The S1 homunculus is clearly visible in a magnified tangential section (Figure 1D; male; P25). Based on our mappings in rats [5], we suspected genital cortex within the dashed square in Figure 1D. Two-photon imaging of this area in Scnn1a-tdTomato mice also showed S1 subfields delineated by septa (Figure 1E). Next, we used intrinsic signal imaging to locate the genital, hindpaw, forepaw, tail, ventral, and dorsal trunk cortex [27, 28]. We sequentially stimulated these body parts with a small circular vibration motor. The resulting intrinsic signal for each body part is shown in Figures 1F and S1. Based on the blood vessel pattern on the surface of the craniotomy (Figure 1G), we aligned these fields. We matched the blood vessel pattern captured during intrinsic imaging with blood vessels captured during two-photon imaging to superimpose intrinsically identified fields onto the pattern of Scnn1a+ neurons in layer 4 (Figure 1H). Intrinsically identified borders between body parts aligned well with septa lacking Scnn1a+ neurons (Figures 1H and S1A) and allowed us

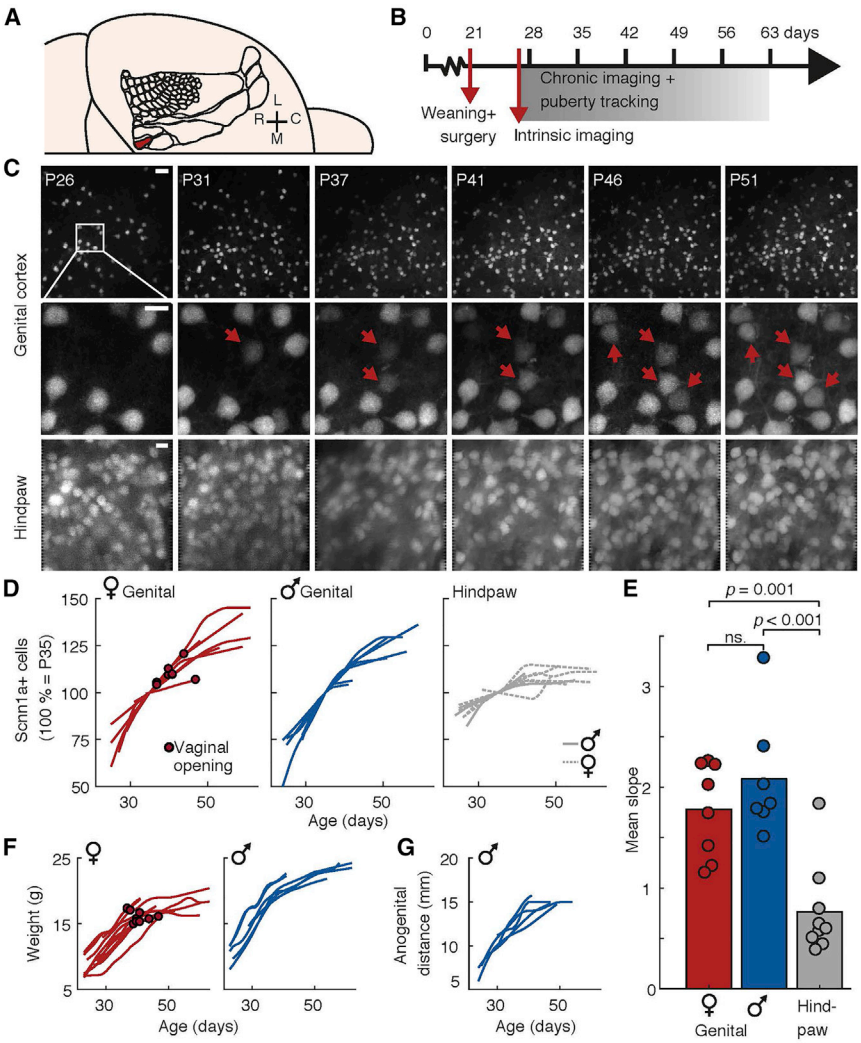

Figure 2. The Number of Scnn1a+ Neurons Increases in Genital Cortex during Puberty

(A) Schematic of the somatosensory homunculus and genital cortex (red).

(B) Experimental timeline for chronic imaging experiments. Mice undergo two-photon imaging sessions every 4–7 days.

(C) Two-photon stacks capturing Scnn1a+ neurons in the same field of view in genital cortex (top) and hindpaw cortex (bottom) between P26 and P51 (from left to right). In genital cortex, additional Scnn1a+ neurons appear over time (middle, arrows). Scale bars: 20 μm (top) and 10 μm (middle, bottom). Arrows mark newly appearing Scnn1a+ neurons.

(D) Scnn1a+ neurons were counted in stacks of genital cortex and hindpaw cortex. Counts are expressed as P35 = 100%. Resulting relative counts increase steeply in female (left; n = 8) and male genital cortex (middle; n = 7) compared to hindpaw cortex (right; gray; n = 9).

(E) The average slope was calculated for each line in (D). The slope of cell counts was greater for female (n = 8; 1.78 ± 0.47) and male (n = 7; 2.30 ± 0.69) genital cortex compared to hindpaw cortex (n = 9; 0.76 ± 0.45; ANOVA; $F(2,21) = 17.2$; $p = 3.73 \times 10^{-5}$; superscripted p values indicate Tukey-Kramer post hoc comparisons).

(F) During chronic imaging experiments, weight of females increased from approximately 8 g to 20 g (left; n = 10) and males reached up to 23 g (right; n = 8).

(G) In males, the anogenital distance increased from 7 mm prepuberty to 16 mm postpuberty (n = 5).

to assign the mouse homunculus to the expression of tdTomato (Figure 1I). Similar to the rat [5], the genital area is located close to the hindpaw. Intrinsic mapping showed very consistent alignment with the pattern of Scnn1a expression (Figures S1B and S1C).

Chronic Imaging of Scnn1a+ Expression across Puberty

To investigate the pubertal development of genital cortex, we conducted chronic two-photon imaging of Scnn1a expression in genital cortex of anesthetized Scnn1a-tdTomato mice (Figure 2A). Mice underwent imaging sessions every 4–7 days starting at the earliest possible time after weaning until early adulthood (approximately P25–P63; Figure 2B). Simultaneously, we tracked pubertal development (see below). Genital and hindpaw cortex were either located using intrinsic signal imaging (Figures 1F–1I) or based on the clear topographic layout Scnn1a expression. During each imaging session, we took a structural z stack of the same field of view (FOV) in genital cortex (Figure 2C, top and middle). Stacks were approximately 200 × 200 μm size and covered the 400 μm between the bottom of L4 and the pia with 2 μm z spacing. Similarly, we acquired stacks of a FOV in hindpaw cortex as a control region (Figure 2C, bottom). Within genital cortex, we observed that some neurons became fluorescent over time (Figure 2C, middle, red arrows), i.e., acquired Scnn1a expression. We counted Scnn1a+ neurons in the acquired series of stacks (Figure 2C, left to right), taking precautions to correct for small shifts in the xy plane or imaging angle (see STAR Methods). The absolute size of the acquired series of stacks varied between mice, depending on the quality of the craniotomy. Therefore, we expressed the resulting cell counts as percentage of the number of cells counted on P35 (5 weeks of age) for both genital and hindpaw cortex. The resulting percentages are then plotted as a line against age for each animal (Figure 2D), always reaching 100% on P35. We found that in genital cortex, the number of Scnn1a+ neurons roughly doubled between weaning and early adulthood in females (Figure 2D, red, left) and males (Figure 2D, blue, middle). In contrast, the number of neurons in hindpaw cortex only increased by ~40% (Figure 2D, gray, right). Next, we calculated the mean slope for each cell count line shown in Figure 2D. To this end, we computed slope at each time point along each line and derived the mean. The mean also included negative values displayed for hindpaw cortex cell counts. The resulting mean slopes for female and male genital cortex as well as hindpaw cortex show that in female and male genital cortex, there are significantly more Scnn1a+ neurons added in comparison to hindpaw cortex

(Figure 2E; slope [mean ± SEM]: female genital [n = 8]: 1.78 ± 0.47; male genital [n = 7]: 2.30 ± 0.69; hindpaw [n = 9]: 0.76 ± 0.45; ANOVA; F (2,21) = 17.2; p = 3.73 × 10^{-5}; p values in Figure 2E indicate Tukey-Kramer pairwise comparisons between female genital cortex, male genital cortex, and hindpaw cortex).

We also tracked the sexual development of mice. Weight increased from ~8 g to ~20 g in females (Figure 2F, left), and males reached up to ~23 g (Figure 2F, right). We monitored vaginal opening in females and anogenital distance (AGD) in males, two markers for pubertal maturation [29, 30]. Vaginal opening occurred around P40 (Figure 2F, left; 40.4 ± 3.1 days). In line with the tight relationship between sexual maturation and weight in females [31], vaginal opening was associated with mice reaching approximately 16 g. In males, the AGD increased from prepubertal 7 mm to adult 16 mm (Figure 2G) [29]. The first ovulation usually occurs 7 days after vaginal opening [32]. In line with this continuous process of sexual maturation, the number of Scnn1a+ neurons did not show a sharp step-like increase. Instead, the increase was gradual, rising steeply before P40 and leveling off toward early adulthood (Figure 2D).

Scnn1a+ Expression Increases while Neuron Density Remains Stable

To determine the origin of newly appearing Scnn1a+ neurons, we performed immunostaining. Tangential brain sections of pre- and postpubertal Scnn1a-tdTomato brains were counterstained with the neuron-selective antibody NeuN conjugated to a green secondary antibody. Fluorescent micrographs show that neither in genital cortex (Figure 3A) nor in hindpaw cortex (Figure 3B) do all L4 neurons (NeuN+, green) express Scnn1a (tdTomato+, red). However, in genital cortex, the number of Scnn1a+ neurons increases from pre- to postpuberty (Figure 3A). We counted the number of Scnn1a+ neurons relative to all neurons (NeuN+) in z stacks (xyz: 100 × 200 × 40 μm; 1 μm z spacing; n = 12 hemispheres) of genital cortex of mice between P24 and P100. Although the percentage of Scnn1a+ neurons increases in genital cortex with age (Figure 3C), it remains stable in hindpaw cortex (Figure 3D). Binning these data into three age groups shows that, in genital cortex (Figure 3E, red), the percentage of Scnn1a+ neurons is significantly lower at prepubertal ages (<P40: 8.47 ± 1.35) compared to postpuberty (P40–P80: 18.0 ± 1.69) and adulthood (>P80: 20.5 ± 2.05), and there was no significant difference between the latter two age groups (ANOVA: F(2,11) = 54.5; p = 9.35 × 10^{-6}; p values in Figure 3E indicate pairwise comparisons between age groups). In comparison, the percentage of Scnn1a+ neurons remains consistently around 60% in hindpaw cortex (ANOVA: F(2,11) = 0.26; p = 0.77; Figure 3E, gray). Finally, neuron density (all NeuN+ per mm^3) is similar and remains stable with age in both genital and hindpaw cortex (Figure 3F). Although the density of Scnn1a+ neurons increases significantly with age, the density of Scnn1a− neurons decreases marginally and not significantly (Pearson's correlation coefficient: Scnn1a+: r = 0.900, p = 0.0001; Scnn1a−: r = −0.133, p = 0.681). These findings are in line with a conversion scenario, where previously Scnn1a− neurons acquire Scnn1a expression during puberty.

Apical Dendrites of Pyramidal Neurons in Genital Cortex Do Not Remodel during Puberty

Within L4, excitatory neurons can be broadly categorized into stellate and pyramidal neurons, defined by the absence and presence of an apical dendrite, respectively [15, 17, 33, 34]. However, at birth, all excitatory L4 neurons appear as pyramids [18], suggesting many retract their apical dendrite to become stellates in the first postnatal week [18]. This process seems to be a hallmark of layer 4 somatosensory map development [19]. To find out whether pyramidal neurons in genital cortex lose their apical dendrite during puberty, we acquired high-magnification two-photon z stacks of neurons within genital cortex of 5 mice. Stacks covered the entire distance from the bottom of L4 to the pia (xyz: 133 × 133 × 400 μm; 2 μm z spacing). We captured the same Scnn1a+ neurons prepuberty (Figure 4A, left top; P30) and postpuberty (Figure 4A, left bottom; P60) and reconstructed all neurons within these stacks (n = 5 pre and 5 post). We identified neurons that were present at both ages and those that newly appeared during adulthood. We further classified each neuron as either stellate (orange) or pyramidal (green) shaped, based on the absence and presence of an apical dendrite, respectively. The high-magnification micrographs (Figure 4A, right) show examples of a pyramidal and a stellate neuron, which evidently do not undergo morphological remodeling during puberty. In fact, 100% of stellate cells (n = 51) retained their stellate cell morphology and 100% of pyramids (n = 63) retained their apical dendrite throughout puberty (Figure 4B). Overall, there were more spiny stellates than pyramids in genital cortex L4 before puberty, and their ratio was not different after puberty (Figure 4C; Fisher's exact test; X^2 = 0.95; p = 0.91).

Stronger Genital-Touch Responses in Layer 4 of Males Compared to Females and a Developmental Increase of Responsiveness in Females

To understand how puberty shapes evoked responses in L4 of genital cortex, we performed calcium imaging of Scnn1a+ neurons during sensory stimulation of the genitals. Three weeks after neonatal injection (P0 to P1), Scnn1a-cre mice showed extensive cre-dependent expression of the activity-dependent calcium indicator flex-GCaMP6s in genital cortex (Figure 5A). Overall, the labeling of Scnn1a+ neurons with flex-GCaMP corresponded well with labeling by genetic crossing of Scnn1a-cre and Ai9-reporter mice (see STAR Methods). For two-photon imaging, mice were lightly anesthetized using isoflurane and head fixed, and genitals were stimulated with a small circular vibration motor for 300 trials (Figure 5B). Care was taken to position the stimulation the exact same way during all experiments (see STAR Methods). For each cell, we computed a $\Delta F/F_0$ trace. Neurons varied in responsiveness to genital stimulation (green dashes, Figure 5C). Because imaging conditions varied, we *Z* scored all traces acquired during a session. To quantify the responsiveness of neurons in genital cortex, we first analyzed all detectable neurons, which also includes Scnn1a+ neurons that acquired Scnn1a expression during puberty. For each cell, we computed a mean Ca^{2+} trace across all trails. The average of these mean traces shows that neurons in males respond more strongly to genital stimulation compared to females (Figure 5D), which is in line with previous findings from rats [5]. Calculating the response index (RI) for male and female neurons ($[F_{max(stim)} - F_{mean(bsl)}]$/ STD ($F_{bsl}$); see STAR Methods)

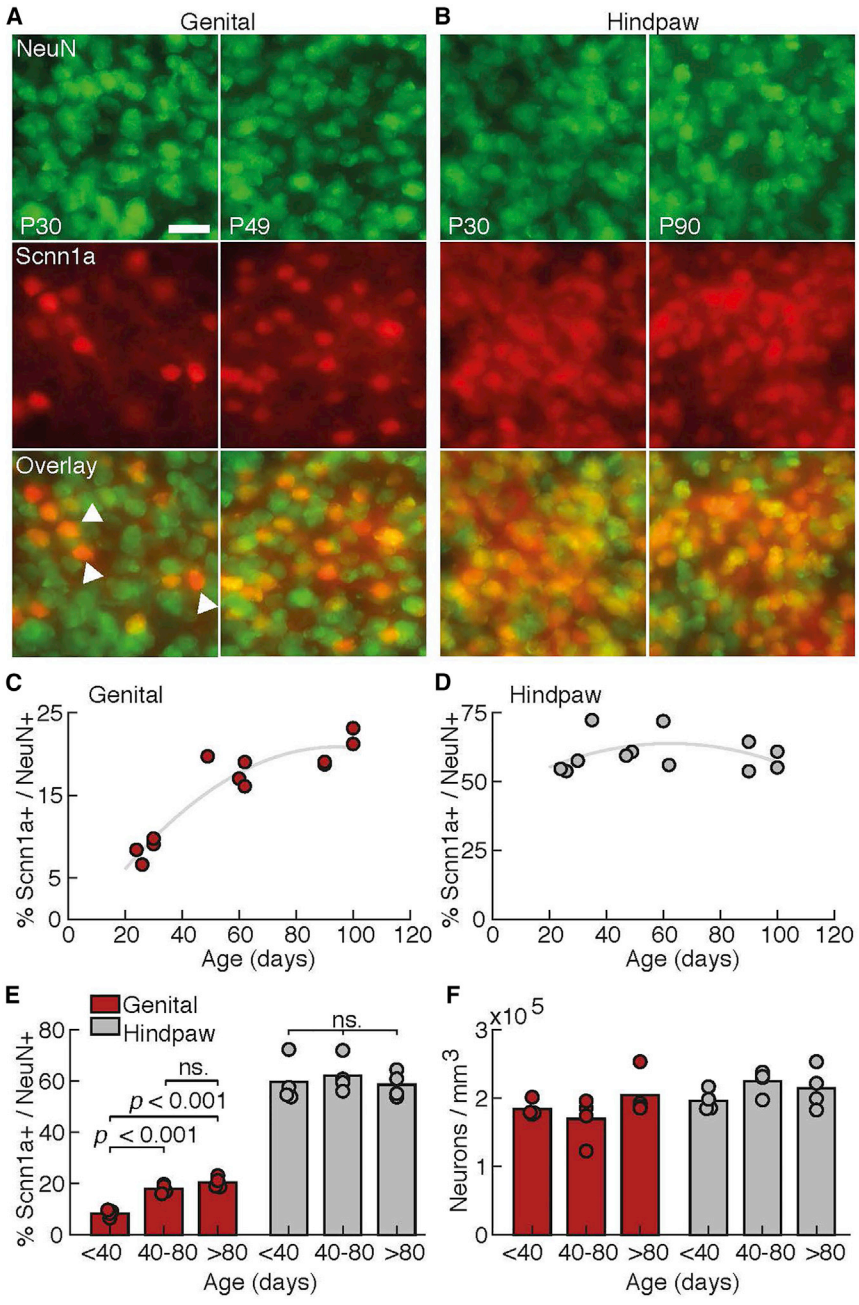

Figure 3. Genital Cortex Scnn1a+ Expression Increases while Neurons Density Remains Stable

(A) Tangential Scnn1a-tdTomato sections (40 μm) of genital cortex layer 4. Sections were stained against NeuN (top, green) to reveal the density of Scnn1a+ neurons (red, middle) relative to all NeuN+ neurons. Scnn1a+ neurons appear as orange in the overlay (white arrows, bottom). Left: prepuberty (P30); right: postpuberty (P49).

(B) Same as (A) but for hindpaw cortex. Left: prepuberty (P30); right: postpuberty (P90). Scale bar (A and B) represents 25 μm.

(C) The number of Scnn1a+ neurons relative to all NeuN+ neurons counted in z stacks of genital cortex plotted against age (days); n = 12 hemispheres. Gray, polynomial fit line.

(D) Same as (C) for hindpaw cortex; n = 12 hemispheres.

(E) Data shown in (C) and (D) binned into three age groups (<P40, P40–P80, and >P80). Left: genital cortex (red); right: hindpaw cortex (gray). p values indicate Tukey-Kramer pairwise comparisons between age groups.

(F) Neuron density per 1 mm^3 for hemispheres shown in (C) and (D). Left: genital cortex (red); right: hindpaw cortex (gray).

showed that this difference was highly significant (RI [mean ± SEM]: males [990 neurons in 5 mice]; 9.02 ± 0.357 versus females [734 neurons in 5 mice]; 5.67 ± 0.124; rank-sum test; Z = 10.2; p = 2.74 × 10^{-24}).

To determine whether response strength changes in genital cortex over the course of puberty, we performed functional imaging experiments between weaning and early adulthood. In females (n = 5), we split neurons according to whether they were recorded before or after vaginal opening. In accordance with previous reports of male puberty onset and the notion that male sexual maturation is independent of weight [31], we used the mean age at vaginal opening (P39) as an approximation in males (n = 5). Evoked responses in males were similar before and after P39 (Figure 5E, top). In contrast, responsiveness increased from before to after vaginal opening in females (Figure 5E, bottom). Accordingly, response indices of prepubertal males were greater than those of prepubertal females (Figure 5E, left; males: n = 551 versus females: n = 465; rank-sum test; $Z = 10.9$; p = 1.04 × 10^{-27}). Furthermore, neurons imaged in adult males responded more strongly to genital stimulation than neurons imaged in adult female mice (Figure 5E, right; males: n = 418 versus females n = 255; rank-sum test; $Z = 2.77$; p = 0.006). Response indices of neurons in genital cortex of males only slightly increased before and after P39 (Figure 5F, top; RI [mean ± SEM]: <P39: 8.79 ± 0.394 versus >P39: 9.45 ± 0.665; rank-sum test; $Z = 1.31$; p = 0.190). In contrast, in females, stimulation of the external genitals elicited significantly larger responses after vaginal opening as compared to before vaginal opening (Figure 5F, bottom; RI [mean ± SEM]: before vaginal opening: 5.24 ± 0.126 versus after vaginal opening: 6.49 ± 0.265; rank-sum test; Z = 4.78; p = 1.74 × 10^{-6}). Given that pubertal maturation is temporally extended, we also correlated the response indices with the age at imaging for males (Figure 5G, top) and females (Figure 5G, bottom). Interestingly, response indices increased with age in females (Pearson's correlation coefficient: r = 0.102; p = 0.006), but not in males (Pearson's correlation coefficient: r = 0.017; p = 0.600). Together, these results show that neurons in genital cortex show sex- and age-dependent response properties.

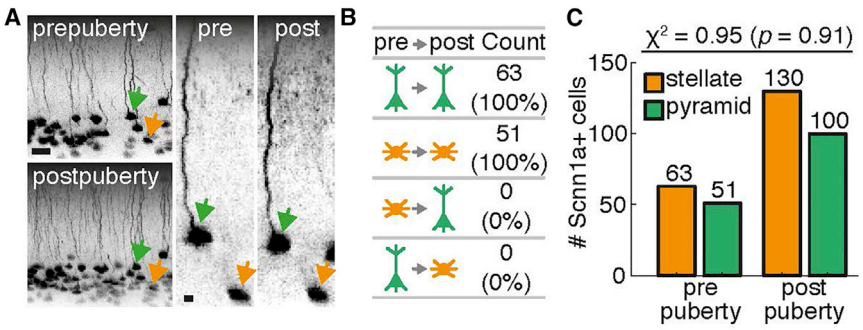

Figure 4. No Evidence for a Loss of Apical Dendrites in Pubertal Development of Scnn1a+ Neuron

(A) Structural stacks (xyz: 133 × 133 × 400 μm; 2 μm z spacing) of Scnn1a+ neurons in genital cortex were vertically reconstructed to reveal dendritic morphology. Stacks of the same FOV were compared pre and postpuberty in 5 mice. There are fewer fluorescent cells prepuberty (left, top) compared to postpuberty (left, bottom). Stellate cells (no apical dendrite; orange arrows) remain stellate cells, and pyramidal cells (with apical dendrite; green arrows) remain pyramidal cells. The same cells are shown at a higher magnification on the right. Scale bars: 50 μm (left) and 10 μm (right).

(B) Scnn1a+ neurons were reconstructed in 5 pre- and 5 postpubertal stacks and identified as stellate or pyramidal shaped. All neurons that were captured before puberty (63 pyramids and 51 stellates in 5 mice) retained their original morphology. No cell underwent a conversion from either stellate to pyramid or vice versa during puberty.

(C) There were slightly more stellates (orange) than pyramids (green) both before (left) and after puberty (right). The number of both stellates and pyramids approximately doubled during puberty. There was no association between age and cell type (Fisher's exact test; $\chi^2 = 0.95$; p = 0.91).

Newly Appearing Scnn1a+ Neurons Respond to Genital Stimulation

Our data suggest that during puberty, many neurons in genital cortex gain Scnn1a+ expression (Figure 2). To determine whether these newly Scnn1a-expressing neurons are functionally active, we performed Ca^{2+} imaging experiments. We identified the newly appearing Scnn1a+ neurons by comparing z stacks acquired before puberty (Figure 6A, top) to stacks acquired postpuberty (Figure 6A, bottom). To ensure that the cellular gain of GCaMP fluorescence after puberty reflected the gain of Scnn1a expression and not a delay in viral transfection, prepubertal stacks were acquired at least 4 weeks after injection. Similar to results observed in Scnn1a-tdTomato mice, many neurons expressed flexed GCaMP6s both before and after puberty (Figure 6A, purple arrows). Other neurons expressed GCaMP only after puberty (Figure 6A, green arrows). We limited our analysis to newly appearing Scnn1a+ neurons that clearly did not express GCaMP before puberty (28 neurons in 2 male and 2 female mice) and compared those to all other recorded neurons (1,689 neurons in 5 male and 5 female mice). The average evoked response of these newly appearing Scnn1a+ neurons was similar to the response evoked in all other neurons (Figures 6B and 6C).

Scnn1a+ and Scnn1a– Neurons Respond Similarly to Genital Stimulation

To determine whether Scnn1a+ and Scnn1a− neurons differ in their responsiveness to genital stimulation, we performed acute two-photon targeted juxtacellular recordings in Scnn1a-tdTomato mice under urethane anesthesia. We visualized L4 of genital cortex using two-photon microscopy and stimulated the external genital region as before (Figure 5). For juxtacellular recordings, we inserted a pipette filled with a green fluorescent dye (Alexa 488) and recorded evoked responses of both putative Scnn1a+ (Figure S2A, red) and putative Scnn1a− neurons, which were identifiable as dark shadows within the fluorescently labeled neuropil (Figure S2A, white arrows). After recording, neurons were electroporated (see STAR Methods) with Alexa Fluor 488 to identify the recorded neuron (Scnn1a+ versus Scnn1a−). Scnn1a− neurons turned from not fluorescent (Figure S2B, top) to green fluorescent after electroporation (Figure S2B, bottom). In contrast, the Scnn1a-tdTomato+ neurons (Figure S2C, top) became red and green after electroporation (Figure S2C, bottom). Labeling efficacy was high (>90%), and multiple cells could be recorded and identified within the same animal (21 identified Scnn1a+ neurons and 25 identified Scnn1a− neurons in 2 males and 4 females). The mean firing rate of Scnn1a− (Figure S2D) and Scnn1a+ neurons (Figure S2E) in response to 200 ms of genital stimulation (shaded gray box) were overall similar. Mean firing rate differences were calculated by subtracting the mean firing rate during the 200 ms preceding stimulus onset from the mean firing rate during genital stimulation (200 ms) for each cell (Figure S2F). Overall, Scnn1a+ neurons responded slightly more strongly to genital stimulation than Scnn1a− neurons, but this difference was not statistically significant (Kruskal-Wallis test; p = 0.154).

Co-housing Prepubertal Females with Adult Males Advances the Gain of Scnn1a+ Neurons in Genital Cortex

Pubertal development of female mice can be accelerated by co-housing them with adult males via the synergistic effect of male pheromones and touch [8]. Specifically, three days of co-housing resulted in a tripling of uterine weight. We have previously shown that this induced advance in pubertal maturation by male conspecifics also accelerates the expansion of genital cortex in prepubertal female rats [6]. Therefore, we wondered whether co-housing with adult males and the concomitant first sexual experience would also accelerate the gain of Scnn1a expression in genital cortex. To test this, we performed chronic imaging experiments of Scnn1a-tdTomato mice similar to Figure 2. Now, female mice were co-housed with sexually mature males between P36 and P39 (Figure 7A). At P36, females had just reached 15 g of bodyweight (Figure 7B), a time point where the uterine response to adult males is maximal [8] although vaginal opening had not yet occurred. Although weight gain was similar between single and co-housed females, vaginal opening occurred slightly, albeit not significantly, earlier in co-housed females (Figure 7C; alone [n = 8]: P40.4 ± P3.1 versus +male [n = 7]: P38.7 ± P1.5 days of age; unpaired

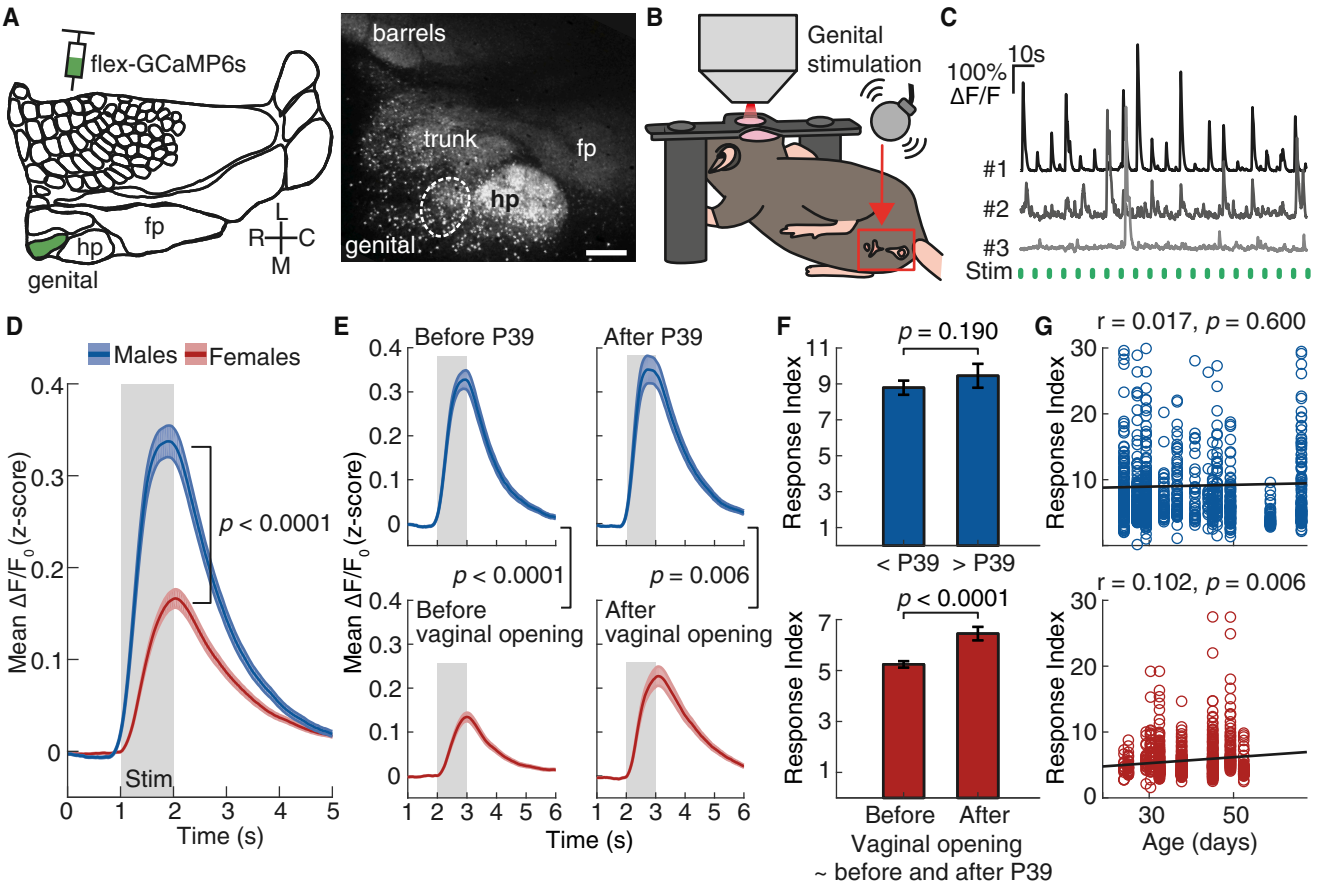

Figure 5. Calcium Imaging Reveals Sex and Development Responses in Genital Cortex

(A) GCaMP expression in S1 of Scnn1a-cre mice. Scale bar represents 250 μm.

(B) Genitals were stimulated with a small vibration motor during Ca^{2+} imaging.

(C) Example Ca^{2+} traces. No. 1: strongly responding; no. 2: weakly responding; no. 3: non-responding. Stimulation, green.

(D) Average evoked Ca^{2+} response in males (blue; 990 neurons) and in females (red; 734 neurons). Shown is the mean (line) and SEM (shaded) of the mean responses of all cells. Response indices (RIs) (see STAR Methods) were greater for males than for females (rank-sum test; $Z = 10.2$; $p = 2.74 \times 10^{-24}$).

(E) Same as (D), split according to age at vaginal opening for females (red). Mean age at vaginal opening (P39) was used as approximation for puberty in males (blue). Prepubertal male neurons (top left; 551 neurons) responded more strongly to genital stimulation than female neurons (bottom left; 465 neurons; rank-sum test; $Z = 10.9$; $p = 1.04 \times 10^{-27}$). This was also true after puberty (right, males: 418 neurons versus females 255 neurons; rank-sum test; $Z = 2.77$; $p = 0.006$).

(F) RIs (mean ± SEM) for males (top) and females (bottom) before and after putative puberty onset. The mean RI increased marginally for males (rank-sum test; $Z = 1.31$; $p = 0.190$) but strongly for females (rank-sum test; $Z = -4.78$; $p = 1.74 \times 10^{-6}$).

(G) Males (top) and female (bottom) genital response indices as a function of age (Pearson's correlation coefficient).

See also Figure S2.

t test; p = 0.209). Scnn1a+ neurons were imaged in genital cortex of co-housed females and counted in series of stacks of the same FOV captured between P25 and P63. In females sitting alone, fewer neurons gained Scnn1a expression between P36 and P39 (Figure 7D) compared to females co-housed with adult males (Figure 7E). We quantified this increase in Scnn1a+ cells for females sitting alone (Figure 7F, left; same as Figure 2D) and for females co-housed with males (Figure 5F, right). A close examination of P36–P39 (Figure 7G) highlights the steep increase in Scnn1a+ neurons for co-housed females in this short time window (Figure 7G, right). Between P36 and P39, the slope of cell counts is significantly steeper for co-housed females compared to single-housed females (Figure 7H; alone [n = 8]: 1.89 ± 0.69 versus +male [n = 7]: 3.91 ± 1.60; unpaired t test; p = 0.006). To examine whether this steep increase during co-housing results in an overall increased number of Scnn1a+ neurons in genital cortex or represents an acceleration of Scnn1a+ expression gain, we compared cell counts at P50 (Figure 7I) 11 days after co-housing ended. Interestingly, there was no difference in the relative cell count of Scnn1a+ neurons between single-housed and co-housed females at this stage (Figure 7I; alone [n = 8]: 127 ± 8 versus +male [n = 7]: 136 ± 9; unpaired t test; p = 0.111). Overall, these data suggest that initial sexual experience has a strong effect on Scnn1a expression. This gain of Scnn1a+ cells appears to reflect an accelerating effect on the maturation rather than a life-long expansion of genital cortex.

To examine whether this effect of co-housing is specific to genital cortex, we also captured series of stacks in the hindpaw cortex of co-housed females and compared those to

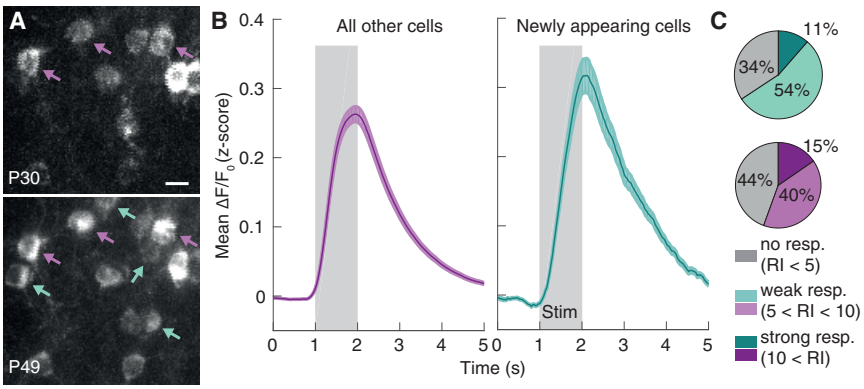

Figure 6. Newly Appearing Scnn1a+ Neurons Respond to Genital Stimulation

(A) Maximum projection of two-photon micrographs of Scnn1a+ neurons in genital cortex expressing GCaMP6s acquired before puberty (P25; top) and after puberty (P49; bottom). In contrast to neurons that can be identified at both time points (purple arrows), there are some neurons appearing as Scnn1a+ at P49 that were not visible at P25 (green arrows, bottom). Scale bar represents 20 μm.

(B) Mean evoked responses of newly appearing Scnn1a+ neurons (right; 28 neurons in 4 mice) and all other imaged neurons (right; 1,689 neurons in 10 mice) to genital stimulation (gray). For each cell, the mean Z scored $\Delta F/F_0$ was computed across trials. Shown is the mean (line) and SEM (shaded) of these mean responses of each cells.

(C) The evoked responses of newly appearing neurons (green) and all other neurons (purple) were classified into three categories according to their RI. Strongly responding: 10 < RI (dark green or purple), weakly responding: 5 < RI < 10 (light green or purple), or non-responding: RI < 5 (gray).

single-house females (Figure S3A). In the hindpaw area, the gain of Scnn1a+ neurons between P36 and P39 is minimal and similar between single and co-housed females (Figure S3B). Similarly, the slope of cell counts within the co-housing period is not different between the two groups in hindpaw cortex (Figure S3C; alone [n = 6]: 1.06 ± 0.82 versus +male [n = 7]: 0.88 ± 0.79; unpaired t test; p = 0.695). Finally, the relative cell count of Scnn1a+ neurons was not different at P50 between co-housed and single-housed females in hindpaw cortex (Figure S3D; alone [n = 6]: 109 ± 4 versus +male [n = 7]: 111 ± 8; unpaired t test; p = 0.668).

DISCUSSION

Our findings reveal that layer 4 of the primary somatosensory genital field undergoes unusually late remodeling during puberty. We showed that the number of Scnn1a+ neurons almost doubles during pubertal maturation and that this gain is gradual rather than stepwise. Our data suggest that within genital cortex, only a fraction of all neurons expresses Scnn1a+ and that this fraction grows during puberty while neuron density is stable. In contrast to developmental processes [18], Scnn1a+ neurons in genital cortex retain their original morphology as stellate or pyramidal neurons. Calcium imaging further showed that neurons in male genital cortex respond more vigorously to genital touch compared to females. It also revealed that newly appearing Scnn1a+ neurons also respond to genital touch. Most interestingly, however, we observed that initial sexual experience drastically accelerated the gain of Scnn1a expression in genital cortex neurons.

During pre- and early postnatal development, extrinsic and intrinsic factors shape the distinct identity of layer 4 primary somatosensory cortex within a brief window of cortical plasticity [35, 36]. Thereafter, the somatosensory homunculus remains particularly stable [9]. Compared to other body parts, genitals significantly change in shape and relevance much later in life [37, 38]. Although recent studies have demonstrated that activity in primary somatosensory cortex does not only reflect the physical properties of touch [39–41], few have yet examined the effect of sexual maturation and, more importantly, sexual experience on the cortical representation of genitals. We specifically targeted layer 4 of genital cortex to build on our previous findings [5–7], although we do not rule out puberty-dependent changes in other layers of genital cortex.

We show that more Scnn1a+ neurons are gained in genital cortex compared to hindpaw cortex and that this increase represents a change in Scnn1a expression and not a gain of new neurons. Scnn1a+ neurons cluster densely in layer 4 of primary somatosensory cortex [19, 22] and pattern it in the shape of the mouse homunculus, suggesting that neurons newly appearing as Scnn1a+ during puberty may resemble a late-acquired layer 4 cell identity. New Scnn1a+ neurons did not appear abruptly but rather gradually, with an initial steep rise that levels off thereafter. This observation is in line with the view that sex hormones act within one temporally extended sensitive period during brain development [42] and not only during one brief perinatal and one brief pubertal pulse [43]. Moreover, we show that initial sexual experience can increase the gain of Scnn1a+ neurons in genital cortex. We suggest that this immediate and drastic effect represents a developmental acceleration rather than a permanent increase, as the relative gain of Scnn1a+ neurons was not different once animals reached adulthood. We wonder whether this imminent accelerating effect of sexual experience on cortical circuitry is related to the great psychological and social significance of initial sexual experience [24, 25], although we cannot exclude the possibility that other kinds of sexual experience (later or premature) also have an effect on genital cortex.

A key property of many excitatory neurons in layer 4 of primary somatosensory cortex is their spiny stellate morphology [18], which depends on the appropriate transcriptional expression [19]. Nevertheless, some excitatory neurons within the granular areas of somatosensory cortex retain their pyramidal morphology [15, 16, 18]. We find that, in genital cortex, there were more spiny stellates compared to pyramids. Although the number of Scnn1a+ neurons almost doubles during sexual maturation in genital cortex, the ratio between stellates and pyramids did not change from prepuberty to postpuberty. We also examined the morphology of pre- and postpubertal Scnn1a+ neurons to find out whether pyramidal Scnn1a+ neurons in genital cortex retract their apical dendrite as some of them do during early development [18]. However, we did not observe any

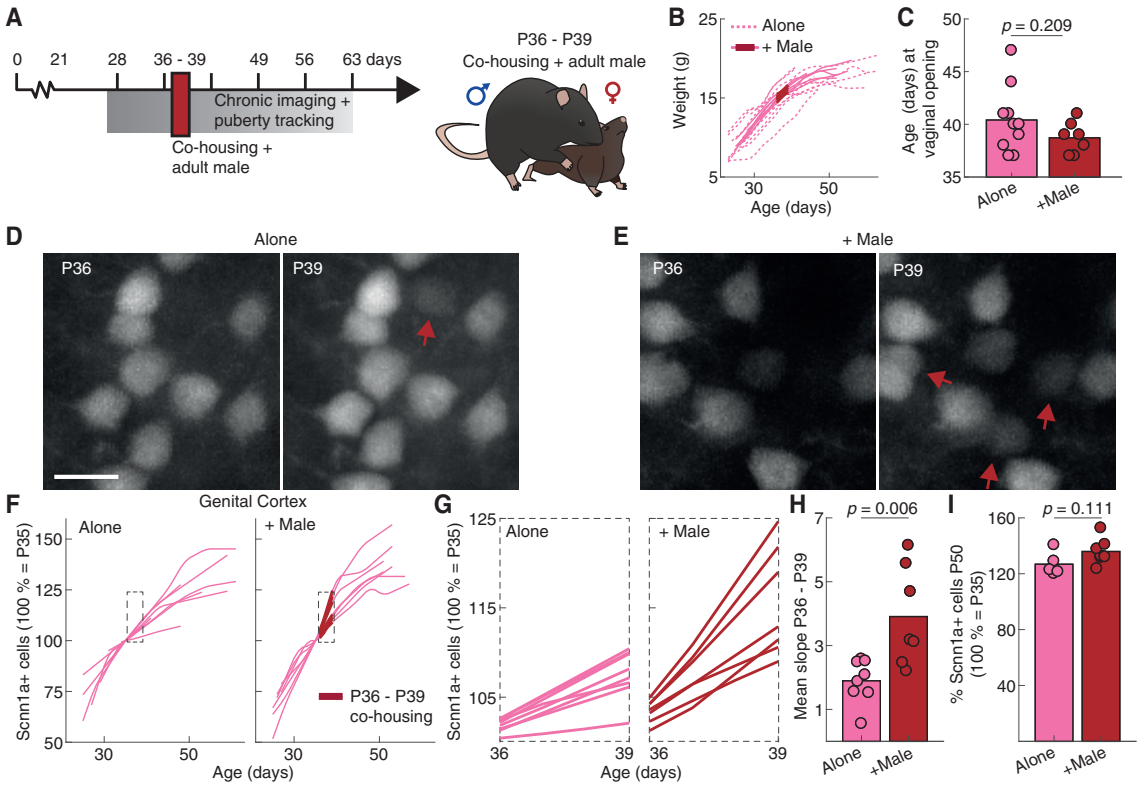

Figure 7. Co-housing Prepubertal Females with Adult Male Mice Advances the Gain of Scnn1a+ Neurons in Genital Cortex

(A) Prepubertal females were co-housed with adult males, when females were between P36 and P39. Chronic imaging was performed as before (Figure 2).

(B) Females sitting alone (dashed pink; n = 10) and females co-housed with males (solid pink; n = 7) gained weight at a similar rate. Co-housing started when female mice reached 15 g and continued for three days (red).

(C) Age at vaginal opening was slightly, but not significantly, advanced in co-housed females (+ male, red, n = 7, 38.7 ± 1.5 versus alone, pink, n = 8, 40.4 ± 3.1; unpaired t test; p = 0.209).

(D) Scnn1a+ neurons in females sitting alone on P36 (left) and P39 (right). Arrows mark newly appearing Scnn1a+ neurons. Scale bar represents 10 μm.

(E) Same as (D) for females co-housed with adult males. Scale bar represents 10 μm.

(F) Scnn1a+ neurons in genital cortex (P35 = 100%) of females sitting alone (left; n = 8; same as Figure 2D) and females co-housed with males (right; n = 7). Days of co-housing, red.

(G) Magnification of dashed boxes in (D). The gain of Scnn1a+ neurons is greater in females sitting with a male (right) compared to females sitting alone (left).

(H) Between P36 and P39, the mean slope of Scnn1a+ cell counts is smaller for single-housed females (left; n = 8; 1.89 ± 0.69) compared to co-housed females (right; n = 7; 3.91 ± 1.60; unpaired t test; p = 0.006).

(I) At P50, relative Scnn1a+ cell counts of females sitting alone (left) and females co-housed with males (right) are not different (unpaired t test; p = 0.111).

See also Figure S3.

pyramidal neurons that retracted their dendrites during this late stage. Alternatively, neurons in genital cortex may have already undergone morphological remodeling just prior to gaining Scnn1a expression. Unfortunately, we cannot investigate this scenario because layer 4 neurons do not express all viral constructs well and can be more easily visualized *in vivo* by using a transgenic mouse line.

Using two-photon calcium imaging, we show that responses of layer 4 neurons in genital cortex to genital touch are more complex than anticipated. Similar to previous observations in rats [5], we found greater responsiveness of genital cortex neurons in males compared to females. In addition, we also observed a positive correlation between age at recording and response strength in females, but not in males. Given that genital cortex appears anatomically monomorphic in males and females, this physiological dimorphism is particularly surprising. Differences in the anatomy of male and female genitals may contribute to this result. In males, the surface area of the external genitals (penis and scrotum) is significantly larger than that of female genitals, where stimulation of the skin, as it is applied here, does not resemble the sensory input that female genitals receive during natural intercourse. Moreover, males are usually heavier than females, possibly resulting in differences in depth of anesthesia. To further elucidate how genital cortex processes sensory inputs in an age-, sex-, and possibly hormone-dependent manner, it will be key do develop approaches to exert precise local (vagina versus clitoris) and naturalistic (external versus internal) sexual stimulation on the female genital tract [44].

Finally, we cannot rule out the possibility that Scnn1a+ constitutes a special subpopulation of layer 4 neurons, at least in genial cortex. Although it would have been of great interest to investigate Scnn1a− neurons *in vivo*, there is currently no feasible strategy to target these neurons optically. Therefore,

we turned to two-photon guided juxtacellular recordings to investigate whether Scnn1a+ and Scnn1a− neurons differ in their response properties to genital stimulation. The results suggested similar response strengths of Scnn1a+ and Scnn1a− neurons. Yet, it is conceivable that our experimental approach was insufficient to resolve differences between these cell types. For one, we cannot rule out that sensory responses of Scnn1a− neurons arise from excitatory network activity. We suggest probing thalamic input to layer 4 more precisely by selectively activating primary thalamic afferents while recording from postsynaptic targets in layer 4. Alternatively, it would also be interesting to selectively label layer 4 neurons that receive thalamic input in Scnn1a-cre mice to find out how these neurons map onto Scnn1a expression. In a similar vein, comparing the molecular profile of Scnn1a+ and Scnn1a− neurons as well as the factors that lead to the gain of Scnn1a+ expression during puberty will be important. For example, hormone-level changes during puberty might influence Scnn1a expression and cellular functions of Scnn1a+ neurons: the Scnn1a gene encodes for the alpha subunit of a well-known non-voltage gated epithelial sodium channel (ENaC) in various organs. Interestingly, the activity of this channel is dependent on estrogen in several tissues [45–47].

Conclusions

In line with earlier observations, our novel results show that layer 4 of genital cortex follows a unique developmental trajectory. Rather than being fully developed after the first postnatal week, many of its principal neurons assume their primary cortex layer 4 cell identity only in the course of puberty. Our data show that genital cortex maturation can dramatically accelerate the initial sexual experience. We wonder if the molding of the genital representation by initial sexual interaction contributes to its huge mnemonic weight and its powerful effects on the perception of one's own sexuality.

STAR★METHODS

Detailed methods are provided in the online version of this paper and include the following:

- KEY RESOURCES TABLE
- LEAD CONTACT AND MATERIALS AVAILABILITY
- EXPERIMENTAL MODEL AND SUBJECT DETAILS
  - Animals
- METHOD DETAILS
  - Assessment of pubertal development
  - Sensory stimulation of the body surface
  - Headpost and window surgery
  - Intrinsic imaging of genital cortex
  - Two-photon imaging
  - Chronic imaging of Scnn1a+ neurons
  - Manipulation of pubertal development
  - Neonatal viral injections
  - Functional 2-photon imaging
  - Targeted Juxta-cellular recording
  - Immunohistochemistry
- QUANTIFICATION AND STATISTICAL ANALYSIS
- DATA AND CODE AVAILABILITY

SUPPLEMENTAL INFORMATION

Supplemental Information can be found online at https://doi.org/10.1016/j.cub.2019.08.062.

ACKNOWLEDGMENTS

We thank Eduard Maier, Constanze Lenschow, and Konstantin Hartmann for comments on the manuscript. We thank Undine Schneeweiß, Juliane Diederichs, and Tanja Wölk for excellent technical assistance. We thank Jean-Sebastien Jouhanneau for advice for targeted juxtacellular recordings. J.S.-G. was funded by the Boehringer Ingelheim Fonds. J.S.-G., E.M., and M.B. were funded by the Humboldt-Universität zu Berlin, BCCN Berlin (German Federal Ministry of Education and Research BMBF, Förderkennzeichen 01GQ1001A), a grant from the DFG (BR 3479/11-1), NeuroCure, and the Gottfried Wilhelm Leibniz Prize of the DFG. M.B., N.T., and M.L. were funded by the Deutsche Forschungsgemeinschaft (DFG, German Research Foundation)—project number 327654276—SFB 1315.

AUTHOR CONTRIBUTIONS

J.S.-G. and M.B. designed the experiments; J.S.-G. and E.M. performed the experiments; N.T. assisted with two-photon imaging and analysis; R.S. and M.L. provided transgenic lines and other equipment; J.S.-G., E.M., and M.B. analyzed the data; and J.S.-G. and M.B. wrote the manuscript.

DECLARATION OF INTERESTS

The authors declare no competing interests.

Received: June 4, 2019
Revised: August 9, 2019
Accepted: August 22, 2019
Published: October 17, 2019

REFERENCES

1. Van der Loos, H., and Woolsey, T.A. (1973). Somatosensory cortex: structural alterations following early injury to sense organs. Science *179*, 395–398.
2. Agmon, A., Yang, L.T., Jones, E.G., and O'Dowd, D.K. (1995). Topological precision in the thalamic projection to neonatal mouse barrel cortex. J. Neurosci. *15*, 549–561.
3. Erzurumlu, R.S., and Jhaveri, S. (1990). Thalamic axons confer a blueprint of the sensory periphery onto the developing rat somatosensory cortex. Brain Res. Dev. Brain Res. *56*, 229–234.
4. Feldman, D.E., and Brecht, M. (2005). Map Plasticity in Somatosensory Cortex (American Association for the Advancement of Science).
5. Lenschow, C., Copley, S., Gardiner, J.M., Talbot, Z.N., Vitenzon, A., and Brecht, M. (2016). Sexually monomorphic maps and dimorphic responses in rat genital cortex. Curr. Biol. *26*, 106–113.
6. Lenschow, C., Sigl-Glöckner, J., and Brecht, M. (2017). Development of rat female genital cortex and control of female puberty by sexual touch. PLoS Biol. *15*, e2001283.
7. Lauer, S.M., Lenschow, C., and Brecht, M. (2017). Sexually selected size differences and conserved sexual monomorphism of genital cortex. J. Comp. Neurol. *525*, 2706–2718.
8. Bronson, F.H., and Maruniak, J.A. (1975). Male-induced puberty in female mice: evidence for a synergistic action of social cues. Biol. Reprod. *13*, 94–98.
9. Kaas, J.H. (1991). Plasticity of sensory and motor maps in adult mammals. Annu. Rev. Neurosci. *14*, 137–167.
10. Gennari, F. (1782). De Peculiari Structura Cerebri Nonnullisque Ejus Morbis (Ex Regio Typographeo).
11. Woolsey, C.N., and Fairman, D. (1946). Contralateral, ipsilateral, and bilateral representation of cutaneous receptors in somatic areas I and

II of the cerebral cortex of pig, sheep, and other mammals. Surgery *19*, 684–702.

12. Pouchelon, G., Gambino, F., Bellone, C., Telley, L., Vitali, I., Lüscher, C., Holtmaat, A., and Jabaudon, D. (2014). Modality-specific thalamocortical inputs instruct the identity of postsynaptic L4 neurons. Nature *511*, 471–474.
13. Moreno-Juan, V., Filipchuk, A., Antón-Bolaños, N., Mezzera, C., Gezelius, H., Andrés, B., Rodríguez-Malmierca, L., Susín, R., Schaad, O., Iwasato, T., et al. (2017). Prenatal thalamic waves regulate cortical area size prior to sensory processing. Nat. Commun. *8*, 14172.
14. Li, H., Fertuzinhos, S., Mohns, E., Hnasko, T.S.S., Verhage, M., Edwards, R., Sestan, N., and Crair, M.C.C. (2013). Laminar and columnar development of barrel cortex relies on thalamocortical neurotransmission. Neuron *79*, 970–986.
15. Staiger, J.F., Flagmeyer, I., Schubert, D., Zilles, K., Kötter, R., and Luhmann, H.J. (2004). Functional diversity of layer IV spiny neurons in rat somatosensory cortex: quantitative morphology of electrophysiologically characterized and biocytin labeled cells. Cereb. Cortex *14*, 690–701.
16. Scala, F., Kobak, D., Shan, S., Bernaerts, Y., Laturnus, S., Cadwell, C.R., Hartmanis, L., Froudarakis, E., Castro, J., Tan, Z.H., et al. (2019). Neocortical layer 4 in adult mouse differs in major cell types and circuit organization between primary sensory areas. bioRxiv. https://doi.org/10.1101/507293.
17. Elston, G.N., Pow, D.V., and Calford, M.B. (1997). Neuronal composition and morphology in layer IV of two vibrissal barrel subfields of rat cortex. Cereb. Cortex *7*, 422–431.
18. Callaway, E.M., and Borrell, V. (2011). Developmental sculpting of dendritic morphology of layer 4 neurons in visual cortex: influence of retinal input. J. Neurosci. *31*, 7456–7470.
19. Klingler, E., De la Rossa, A., Fièvre, S., Devaraju, K., Abe, P., and Jabaudon, D. (2019). A translaminar genetic logic for the circuit identity of intracortically projecting neurons. Curr. Biol. *29*, 332–339.e5.
20. Vue, T.Y., Lee, M., Tan, Y.E., Werkhoven, Z., Wang, L., and Nakagawa, Y. (2013). Thalamic control of neocortical area formation in mice. J. Neurosci. *33*, 8442–8453.
21. Madisen, L., Zwingman, T.A., Sunkin, S.M., Oh, S.W., Zariwala, H.A., Gu, H., Ng, L.L., Palmiter, R.D., Hawrylycz, M.J., Jones, A.R., et al. (2010). A robust and high-throughput Cre reporting and characterization system for the whole mouse brain. Nat. Neurosci. *13*, 133–140.
22. De la Rossa, A., Bellone, C., Golding, B., Vitali, I., Moss, J., Toni, N., Lüscher, C., and Jabaudon, D. (2013). In vivo reprogramming of circuit connectivity in postmitotic neocortical neurons. Nat. Neurosci. *16*, 193–200.
23. Oishi, K., Aramaki, M., and Nakajima, K. (2016). Mutually repressive interaction between Brn1/2 and Rorb contributes to the establishment of neocortical layer 2/3 and layer 4. Proc. Natl. Acad. Sci. USA *113*, 3371–3376.
24. Bozon, M., and Kontula, O. (1998). Sexual initiation and gender in Europe: a cross-cultural analysis of trends in the twentieth century. In Sexual Behaviour and HIV/AIDS in Europe: Comparisons of National Surveys, N. Bajos, M. Hubert, and T. Sandfort, eds. (Routledge), p. 37.
25. Simon, W. (2017). Sexual Conduct: The Social Sources of Human Sexuality (Routledge).
26. Lein, E.S., Hawrylycz, M.J., Ao, N., Ayres, M., Bensinger, A., Bernard, A., Boe, A.F., Boguski, M.S., Brockway, K.S., Byrnes, E.J., et al. (2007). Genome-wide atlas of gene expression in the adult mouse brain. Nature *445*, 168–176.
27. Palmer, L.M., Schulz, J.M., Murphy, S.C., Ledergerber, D., Murayama, M., and Larkum, M.E. (2012). The cellular basis of GABA(B)-mediated interhemispheric inhibition. Science *335*, 989–993.
28. Grinvald, A., Lieke, E., Frostig, R.D., Gilbert, C.D., and Wiesel, T.N. (1986). Functional architecture of cortex revealed by optical imaging of intrinsic signals. Nature *324*, 361–364.
29. Divall, S.A., Williams, T.R., Carver, S.E., Koch, L., Brüning, J.C., Kahn, C.R., Wondisford, F., Radovick, S., and Wolfe, A. (2010). Divergent roles of growth factors in the GnRH regulation of puberty in mice. J. Clin. Invest. *120*, 2900–2909.
30. Safranski, T.J., Lamberson, W.R., and Keisler, D.H. (1993). Correlations among three measures of puberty in mice and relationships with estradiol concentration and ovulation. Biol. Reprod. *48*, 669–673.
31. Falconer, D.S. (1984). Weight and age at puberty in female and male mice of strains selected for large and small body size. Genet. Res. *44*, 47–72.
32. Gaytan, F., Morales, C., Leon, S., Heras, V., Barroso, A., Avendaño, M.S., Vazquez, M.J., Castellano, J.M., Roa, J., and Tena-Sempere, M. (2017). Development and validation of a method for precise dating of female puberty in laboratory rodents: the puberty ovarian maturation score (pubscore). Sci. Rep. *7*, 46381.
33. Brecht, M., and Sakmann, B. (2002). Dynamic representation of whisker deflection by synaptic potentials in spiny stellate and pyramidal cells in the barrels and septa of layer 4 rat somatosensory cortex. J. Physiol. *543*, 49–70.
34. Guillamon-Vivancos, T., Tyler, W.A., Medalla, M., Chang, W.W., Okamoto, M., Haydar, T.F., and Luebke, J.I. (2019). Distinct neocortical progenitor lineages fine-tune neuronal diversity in a layer-specific manner. Cereb. Cortex *29*, 1121–1138.
35. Antón-Bolaños, N., Espinosa, A., and López-Bendito, G. (2018). Developmental interactions between thalamus and cortex: a true love reciprocal story. Curr. Opin. Neurobiol. *52*, 33–41.
36. Simi, A., and Studer, M. (2018). Developmental genetic programs and activity-dependent mechanisms instruct neocortical area mapping. Curr. Opin. Neurobiol. *53*, 96–102.
37. Han, S.H., and Lee, S.-H. (2013). Differential growth of the reproductive organs during the peripubertal period in male rats. Dev. Reprod. *17*, 469–475.
38. Tomova, A., Deepinder, F., Robeva, R., Lalabonova, H., Kumanov, P., and Agarwal, A. (2010). Growth and development of male external genitalia: a cross-sectional study of 6200 males aged 0 to 19 years. Arch. Pediatr. Adolesc. Med. *164*, 1152–1157.
39. Lenschow, C., and Brecht, M. (2015). Barrel cortex membrane potential dynamics in social touch. Neuron *85*, 718–725.
40. Bobrov, E., Wolfe, J., Rao, R.P., and Brecht, M. (2014). The representation of social facial touch in rat barrel cortex. Curr. Biol. *24*, 109–115.
41. Ishiyama, S., and Brecht, M. (2016). Neural correlates of ticklishness in the rat somatosensory cortex. Science *354*, 757–760.
42. Schulz, K.M., and Sisk, C.L. (2016). The organizing actions of adolescent gonadal steroid hormones on brain and behavioral development. Neurosci. Biobehav. Rev. *70*, 148–158.
43. Sisk, C.L., and Zehr, J.L. (2005). Pubertal hormones organize the adolescent brain and behavior. Front. Neuroendocrinol. *26*, 163–174.
44. Adler, N.T., Davis, P.G., and Komisaruk, B.R. (1977). Variation in the size and sensitivity of a genital sensory field in relation to the estrous cycle in rats. Horm. Behav. *9*, 334–344.
45. Greenlee, M.M., Mitzelfelt, J.D., Yu, L., Yue, Q., Duke, B.J., Harrell, C.S., Neigh, G.N., and Eaton, D.C. (2013). Estradiol activates epithelial sodium channels in rat alveolar cells through the G protein-coupled estrogen receptor. Am. J. Physiol. Lung Cell. Mol. Physiol. *305*, L878–L889.
46. Yusef, Y.R., Thomas, W., and Harvey, B.J. (2014). Estrogen increases ENaC activity via PKCδ signaling in renal cortical collecting duct cells. Physiol. Rep. *2*, e12020.
47. Yang, G.Z., Nie, H.G., Lu, L., Chen, J., Lu, X.Y., Ji, H.L., and Li, Q.N. (2011). Estrogen regulates the expression and activity of epithelial sodium channel in mouse osteoblasts. Cell. Mol. Biol. *57* (*Suppl*), OL1480–OL1486.
48. Pachitariu, M., Stringer, C., Dipoppa, M., Schröder, S., Rossi, L.F., Dalgleish, H., Carandini, M., and Harris, K.D. (2017). Suite2p : beyond

10, 000 neurons with standard two-photon microscopy. bioRxiv. https://doi.org/10.1101/061507.

49. Kim, J.-Y., Grunke, S.D., Levites, Y., Golde, T.E., and Jankowsky, J.L. (2014). Intracerebroventricular viral injection of the neonatal mouse brain for persistent and widespread neuronal transduction. J. Vis. Exp. 51863.

50. Takahashi, N., Oertner, T.G., Hegemann, P., and Larkum, M.E. (2016). Active cortical dendrites modulate perception. Science *354*, 1587–1590.

51. Judkewitz, B., Rizzi, M., Kitamura, K., and Häusser, M. (2009). Targeted single-cell electroporation of mammalian neurons in vivo. Nat. Protoc. *4*, 862–869.

STAR★METHODS

KEY RESOURCES TABLE

REAGENT or RESOURCE	SOURCE	IDENTIFIER
Bacterial and Virus Strains		
pAAV-Syn-Flex-GCaMP6s-WPRE	Addgene	Cat #: 100843
Antibodies		
Anti-NeuN antibody, monoclonal, anti-mouse	Millipore	Cat #: MAB377; RRID: AB_2298772
Donkey Anti-Mouse IgG, Alexa Fluor 488	Thermofisher	Cat #: R73114; RRID: AB_2556542
Chemicals, Peptides, and Recombinant Proteins		
Alexa Fluor 488 Hydrazide	ThermoFisher	Cat #: 10463
Experimental Models: Organisms/Strains		
Mouse: B6;C3-Tg(Scnn1a-cre)3Aibs/J *Mus musculus*	JAX	Cat #: 009613; RRID: IMSR_JAX:009613
Mouse: B6.Cg-Gt(ROSA)26Sor$^{tm9(CAG-tdTomato)Hze}$/J *Mus musculus*	JAX	Cat #: 007909; RRID: IMSR_JAX:007909
Mouse: C57BL/6JRj	Janvier	N/A
Software and Algorithms		
ImageJ	NIH	https://imagej.nih.gov/ij/
MATLAB	Mathworks	https://de.mathworks.com/products/matlab.html
Adobe Illustrator	Adobe	https://www.adobe.com
Spike2	CED	http://ced.co.uk/products/spkovin
Suite2p	[48]	https://github.com/MouseLand/suite2p

LEAD CONTACT AND MATERIALS AVAILABILITY

This study did not create new unique reagents or mouse lines. Further information and requests for resources and reagents should be directed to and will be fulfilled by the Lead Contact, Michael Brecht, michael.brecht@bccn-berlin.de.

EXPERIMENTAL MODEL AND SUBJECT DETAILS

Animals

All experimental procedures were performed according to the German guidelines on animal welfare under the supervision of local ethics committee (animal permit number G0244/16). Adult Scnn1a-Tg3-Cre (B6;C3-Tg(Scnn1a-cre)3Aibs/J, RRID: IMSR_JAX:009613) and Ai9-reporter mice (B6;Cg-Gt(ROSA)26Sor$^{tm9(CAG-tdTomato)Hze}$/J, RRID: IMSR_JAX:007909) mice were purchased from Jackson Labs. Wild-type C57BL/6JRj mice were purchased from Janvier. For intrinsic and chronic imaging, juxta cellular experiments and histology, heterozygous Scnn1a-cre mice were bred with homozygous Ai9-reporter mice. Scnn1a x Ai9 positive offspring constitutively expressed tdTomato in all cre-positive cells (Scnn1a-tdTomato). Males and females between postnatal day (P) 25 and P90 were used. For calcium imaging experiments, we used single transgenic Scnn1a-cre mice injected with flexed GCaMP6s. All animals were weaned at P20 and genotyped by Transnetyx (Cordova, TN). Mice were housed alone or in pairs under a 12-hour light and dark cycle in temperature controlled cabinets with *ad libitum* chow and water.

METHOD DETAILS

Assessment of pubertal development

Throughout chronic experiments (P25 - P60), weight and external parameters of pubertal development were closely monitored. Weights were smoothed with a three day sliding window and plotted across days for each animal. Females were inspected daily starting at weaning to record vaginal opening. For males, we recorded the distance between anus and penis (anogenital distance, AGD). Both, vaginal opening and AGD are dependent upon the activation of the hypothalamic-pituitary-gonadal axis [29].

Sensory stimulation of the body surface

For stimulation of the body surface, in particular the external genitals, we used a small circular vibration motor, usually found in mobile phones (Ø 8 mm, 3 mm thick, Eckart Electronics, PO1637), which emits 10 Hz vibrations. The vibration motor was attached to a costume made control box, which could be triggered by TTL pulses during intrinsic imaging, two-photon calcium imaging and

juxtacellular recordings. The vibration motor was held by a micro-manipulator which allowed precise positioning on the genital or other body parts. To stimulate the genital in males, the vibration motor was positioned on top of the penis and the scrotum. In females, it was positioned to cover the exit of the urethra, the clitoris and the vulva.

Headpost and window surgery

For all chronic imaging experiments, mice underwent headpost and window surgeries following weaning approximately at P25. Mice were anaesthetized with isoflurane (1.5 – 2% in O2). Body temperature was maintained at 36°C using a heatpad. After removing the skin covering the skull, a circular 3 mm craniotomy was made positioned between the coronal suture and the midline. The dura was left intact and the craniotomy was sealed with a stack of three coverslips, 3 mm, 3 mm and 4 mm glued together with light Norland optic adhesive 71 (Norland products) and affixed using superglue. A light-weight, two-point fixation headpost was glued on the skull surrounding the craniotomy, before sealing everything with dental cement.

Intrinsic imaging of genital cortex

Topographic maps in S1 were functionally identified using intrinsic optical imaging (iOS) as previously described [27, 28]. For this purpose, mice were lightly anesthetized with isoflurane (0.5 – 1% in O2) and placed on a heatpad. We sequentially identified several body parts in each mouse which included the genital, hindpaw, forepaw, genital, tail, ventral and dorsal trunk. To limit the duration of anesthesia per experiment not all body parts were mapped in all mice. For identifying each body part, we placed the small circular vibration motor on it using a micromanipulator. Care was taken to prevent the vibration motor to touch anything but the body part under investigation. To reach the ventral side of the paws, they were minimally suspended. To reach the ventral trunk and the genital, the lower body was slightly twisted. After appropriate positioning, the blood vessel pattern on the surface of the craniotomy was captured using green illumination (530 nm). Next, the craniotomy was illuminated by a ring of small red LEDs (600 nm) mounted around the objective. Illumination was set so that the craniotomy was homogenously enlightened without saturation. Images were captured using a CCD camera coupled to a 50 nm and 25 nm lens. The signal was measured before and during sensory stimulation (1 s stimulation, 5 s ISI) for 20 sweeps. The intrinsic signal was measured as the difference between reflected light before and during stimulation and was mapped onto the blood vessel pattern (Figure 1F). The signal was then analyzed using ImageJ. Images were converted to gray scale and smoothed using a Gaussian filter (sigma = 10). The area of evoked activity was identified by thresholding the image to binary black and white, where the darkest pixels (strong activity) appeared as black and the remaining image in white. The threshold was set so that pixels within the darkest 10% of the gray scale appeared in black. The resulting fields of activation were superimposed into the blood vessel pattern of the craniotomy (Figure 1G).

Two-photon imaging

Imaging was performed with a Thorlabs B-Scope or a costume built resonant scanning two-photon microscope equipped with GaAsP photomultiplier tubes (assembled by INSS, UK). tdTomato and GCaMP6s were excited at 940 nm (typically 30 to 40 mW at the sample) with a Ti:Sapphire laser (Spectra Physics) and imaged through a 16x 0.8 NA water immersion objective. Images (512 × 512 pixels) were acquired at 30 Hz using ScanImage software. During all imaging experiments, mice were lightly anaesthetized using isofluorane (0.5%–1.0% in O2) and body temperature was maintained using a heatpad.

Chronic imaging of Scnn1a+ neurons

Following window and headpost surgery, animals were allowed to recover for two days. In order to quantify Scnn1a+ cells in L4 of genital cortex, two-photon imaging carried out in Scnn1a-tdTomato transgenic mice, were excitatory neurons in L4 express tdTomato. Starting around P25, mice were imaged at least once per week until approximately 60 days of age. The exact start and endpoint of chronic imaging experiments varied between animals, depending on the quality of the craniotomy. Genital cortex was first identified either using intrinsic imaging (in 9 mice) or the topographic layout of the body map within L4, which is clearly visible in Scnn1a-tdTomato mice used here. To provide an overview of the whole genital field (1065 μm x 1065 μm), a stack was taken at minimal magnification first. Next, a representative subfield was captured at high magnification (~200 μm x 200 μm), which was used to quantify fluorescent cells. In addition, a similar stack was acquired in the somatosensory hindpaw cortex to serve as a control area. Care was taken to capture stacks at the center of the genital or hindpaw area. Stacks were always taken at the same angle and a two-point fixation headpost was used to minimize shifts in the imaging angle. To achieve optimal structural resolution, 60 to 200 images were acquired per z-plane and averaged online. Z stacks were acquired starting below layer 4, densely populated by tdTomato+ neurons, moving upward toward the pia. Stacks covered an overall distance of 400 μm with individual z-planes acquired every 2 μm. Following the first imaging day, the exact same field of view was captured on subsequent imaging days. Image stacks were analyzed using ImageJ as follows: Acquired z stacks were first minimally cropped in the xy-plane to ensure that they included the same FOV across days. With regards to the z axis (depth), neurons were neither cut at the top or bottom due to the large vertical distance that they covered. Cells bodies were then traced by hand throughput the z stacks to quantify the number of fluorescent cells in the genital and hindpaw region throughout puberty. Only neurons that were fully included in the stacks were counted. After counting, we took additional precautions to account for small shifts in the imaging angle, which resulted in Scnn1a+ neurons moving in and out of the stacks across time points. To avoid biases in counting such cells, we created maximum projections of the z stacks after counting cells and made sure that the same neurons were systematically included or excluded. Because stacks were not exactly of the same xy-area (due to posthoc alignment or issues with the quality of the craniotomy), cell counts for each animal are expressed relative to the number of cells counted on P35 (7 weeks).

For morphological classification of Scnn1a+ neurons we captured structural z stacks as described above (xyz: ~133 × 133 × 400 μm, 2 μm z-spacing). In 5 mice we acquired z stacks of the same FOV in genital cortex around P30 and around P60. Stacks were reconstructed in 3D using ImageJ to reveal apical dendrite morphology between L4 and the pial surface. Scnn1a+ positive neurons were classified as either pyramidal or stellate cells, depending on the presence or absence of an apical dendrite, respectively. We further distinguished between neurons that were Scnn1a+ already before puberty (visible at P30 and P60) and those that only appeared after puberty (P60 only).

Manipulation of pubertal development

For manipulation experiments, female mice underwent chronic imaging sessions as described above. In addition, mice were co-housed with sexually mature wild-type mice for three days just prior to onset of puberty. Co-housing started once mice reached a weight of 15 g [8] which occurred at P36. Males were removed again three days later on P39.

Neonatal viral injections

For functional imaging of Scnn1a neurons during puberty, we injected neonatal Scnn1a-cre mice (P0 – P3) with pAAV-Syn-Flex-GCaMP6s-WPRE (Addgene plasmid #100843, RRID: Addgene_100843). For injections, cryoanesthesia was induced by placing pups wrapped in a lab glove on a metal plate on ice for 10 minutes, taking care to avoid pups directly contacting the ice [49]. Pups were positioned dorsal side up, lightly fixed using an adhesive bandage. AAV injections were made using a 10 μL Hamilton syringe (Hamilton) and a 32 gauge needle. For injections the head was held gently and the tip of the needle was inserted carefully through skin and cranium. Between 3 and 5 injections (~50 nl) were made into the left hemisphere directly below the cranium, covering the area between Bregma and Lambda close to the midline (visible through the skin) to cover S1. Pups recovered on a heat pad and were returned to their home cage once awake and re-warmed. All pups survived this procedure and dams did not reject any pups. Pups were weaned at P21 and underwent head-post implantation and window surgery as described above.

Functional 2-photon imaging

Following neonatal injections, two-photon calcium imaging was used to capture sensory evoked activity of Scnn1a+ L4 neurons expressing GCaMP6s throughout puberty. Mice were imaged between 25 and 60 days of age, whereby we sampled different neurons within mice during multiple imaging session. Despite the long duration of GCaMP6s expression, only few cells acquired nuclear filling. Those were excluded from the analysis. Furthermore, we ensured that viral injection of flex-GCaMP6s labeled the same neurons as genetic crossing of Scnn1a-cre and Ai9- reporter mice (resulting in td-Tomato expression). Injecting flex-GCaMP6s in Scnn1a-tdTomato mice showed a good, albeit not perfect, correspondence between both transfection strategies (td-Tomato + GCaMP double labeling: 85.9 ± 2.1%, td-Tomato only: 3.7 ± 2.1%, GCaMP only: 10.4 ± 2.1%).To identify newly appearing Scnn1a+ neurons during adulthood, we took z stacks at 840nm at a prepubertal time point, to be able to identify all neurons that already expressed Scnn1a. During each imaging session, we imaged neurons in the genital while stimulating the external genital with a small vibration motor (see above), triggered by TTL pulses. Time-series movies were acquired at 30 Hz and aligned with stimulations using Spike2 software. The vibration motor was held by a micromanipulator and placed either on the genital area. During each trial, calcium activity was recorded for 2 s (baseline), followed by 1 s of stimulation and a 5 s inter-trial-interval. During each session, we recorded ~300 trials. Calcium traces were extracted using the Suite2p software [48], which performs motion correction and provides neuropil traces for each cell. Automated cell detection by the suite2p software was hand curated. This software uses adequate levels of Ca^{2+} fluorescence as a criterion for detecting neurons. Neurons that acquired nuclear filling by GCaMP6s were therefore automatically disregarded by the algorithm, which was confirmed during hand curation. Neuropil signals were weighed with a factor of 0.7 and subtracted for each cell. The fluorescent change ($\Delta F/F_0$) was calculated as $(F - F_0) / F_0$ where F_0 was the baseline fluorescence value in the ROI throughout the whole imaging session [50]. To account for differences in imaging quality across days, we z-scored all traces acquired during one session and pooled traces afterward across sessions. This ensures that the structure within an imaging session is retained while particularly good or bad imaging sessions cannot distort the overall result. For analysis of event-related calcium activity, we further normalized traces for individual trials by subtracting a baseline comprising the mean fluorescence during the 50 frames preceding the stimulus onset from the entire trial. A response index was calculated for each trial by dividing the maximum $\Delta F/F_0$ during the stimulus by the standard deviation of the 10 frames preceding stimulus onset.

Targeted Juxta-cellular recording

Targeted juxtacellular experiments were carried out using Scnn1a-tdTomato (5 females, 2 males, P25 to P41) transgenic mice. The above surgical protocol for headpost and window implantation was slightly adjusted. On the day preceding the experiment, mice underwent headpost surgery while leaving the skull intact. After implantation, mice were placed under the 2-photon microscope and the topographic layout of L4 (tdTomato positive) was captured by imaging through the skull. On the day of the experiment, mice were anesthetize with 10% urethane (0.01 g/g i.p.). A small craniotomy (1 mm diameter) was made above genital cortex and the dura was removed. Mice were placed under the two-photon microscope, where the body temperature was maintained at 36°C using a rectal probe and a homeothermic blanket (FHC). For sensory stimulation, the vibration motor was positioned on the genital. For simultaneous imaging and electrophysiology, the two-photon objective was positioned at 73° relative to the recording stage. The pipette for juxtacellular recording was controlled by micromanipulators (SM6, Luigs & Neumann) and positioned at 45°

relative to the recording stage. Pipettes (4 - 6 MOhm; pulled with P-97; Sutter Instrument) were filled with intracellular solution containing the following (in mM): K-gluconate 130, Na-gluconate 10, HEPES 10, phosphocreatine 10, Mg-ATP 4, GTP 0.3, NaCl 4 and Alexa 488 hydrazine 10 (ThermoFisher, #10436) at pH 7.2.

We first visualized the pipette tip with the two-photon microscope above the pia, before lowering it down to the surface of the brain, 400-500 μm medial of genital cortex, were we set the vertical micromanipulator to 0. Following insertion into the brain, the pipette was lowered in 3-μm steps until it reached genital cortex layer 4, which was identified by simultaneous two-photon imaging. Once the pipette was positioned in reach of cells of interest, the craniotomy was covered with 1% agarose to improve recording stability and a 3 mm circular glass coverslip for better visibility. We approached Scnn1a+ (tdTomato +) and Scnn1a– (visible as black holes within the tdTomato + neuropil) in an alternating fashion. The distance from the pipette tip to a cell was visualized using two-photon microscopy and monitored by current step (1 nA)-induced voltage deviations, resulting from an increased resistance at the tip of the pipette in the proximity of cells. Cells were recorded in current-clamp mode. Once spike signals were between 0.5 mV and 1.5 mV, stimuli were delivered every 2 s with 200 ms stimulation length for 50 trials. After recording, cells were labeled by applying one 1 s long electroporation pulse train (−10V, 0.5 ms pulse width, 20 ms inter-pulse interval). This labeling procedure was adapted from Judkewitz et al., 2009 [51]. However, distance of the pipette tip to the cell was kept as close as during juxtacellular recording as long-term survival of the cell was not necessary and labeling success was > 90% with this protocol. The labeling procedure was captured using two-photon microscopy: If the labeled neuron at the pipette tip was previously red and appeared yellow after electroporation with Alexa 488 hydrazine, it was classified as a Scnn1a + neuron. If it was non-fluorescent during recording and turned green upon electroporation, it was identified as a Scnn1a - neuron. We excluded recordings with unsuccessful or ambiguous labeling attempts or if two or more cells were labeled. Overall we recorded 21 Scnn1a + and 28 Scnn1a - neurons in 2 males (P25 and P41) and 4 females (2 x P25, P34 and P38), with a similar number of both cell types recorded in each mouse. The recorded signal was amplified by a patch-clamp amplifier (ELC-03XS; NPI, Tamm, Germany) and sampled at 50 kHz by a Power1401 analog to digital converter under the control of Spike2 software (CED). Recordings were analyzed in MATLAB 2015a (MathWorks, MA) using descriptive statistical methods.

Immunohistochemistry

At the end of the above described experiment, animals were anaesthetized using 20% urethane solution and perfused with phosphate buffer followed by 4% paraformaldehyde solution (PFA). Brains were removed, hemispheres were separated, subcortical brain areas removed and cortices were flattened between two glass slides separated by clay spacers. Glass slides were weighed down with small ceramic weights for 3 h. Afterward, flattened cortices were left free floating in 4% PFA overnight. On the next day, PFA was replaced with a 30% sucrose solution for cryoprotection. Afterward, brains were embedded and 40 μm sections were cut on a freezing microtome.

For quantifying the density of Scnn1a+ neurons relative to all other neurons, which were stained with an antibody against the neuron specific protein NeuN. Briefly, sections were washed four times for 10 minutes in 1XPBS and then incubated in a blocking solution containing 1XPBS and 0.5% Triton X-100 (PBS-X) and 10% goat serum for two hours at room temperature. Next, free-floating sections were incubated in the primary antibody mouse anti-NeuN (Millipore, Darmstadt, Germany) diluted (1:1000) in a solution containing PBS-X, 1% BSA and 10% goat serum for at least 24 h under mild shaking at 4°C. Washing sections in 1XPBS was followed by incubation with the secondary antibody (donkey anti-mouse Alexa Fluor 488, Technologies, Darmstadt, Germany) diluted (1:500) in PBS-X and 2% goat serum for at least 24 h in the dark. Finally, sections were mounted on gelatine coated glass slides with Fluoromount mounting medium.

An epifluorescence microscope (DM5500B, Leica Microsystems, Mannheim, Germany) equipped with a camera was used to acquire z stacks of immunofluorescently labeled sections. Fluorophores were excited using the appropriate filter cubes (Alexa 488: L5, tdTomato: N3). Fluorescent images were acquired with a 100x oil-immersion objective. NeuN+ and Scnn1a+ neurons were counted in z stacks of genital and hindpaw cortex layer 4 (xyz: 100 × 200 × 40 μm, 1 μm z-spacing) using the ROI-manager in ImageJ.

QUANTIFICATION AND STATISTICAL ANALYSIS

Data were analyzed in MATLAB (MathWorks, Natick, MA) and are shown as mean ± SEM. The sample size (n) refers to either mice, neurons or hemispheres. Details are provided where appropriate. To quantify the overall increase in the Scnn1a+ neurons in Figure 2E, we applied the MATLAB gradient function to the increase for each mouse plotted in Figure 2D. This function provides the gradient at each time point. These values (both positive and negative) were then averaged to provide the mean slope. Data was tested for normality using the Lilliefors test. Normally distributed data was compared using an unpaired t test or an ANOVA for comparing two or more groups respectively. Non-normally distributed data were analyzed using Rank-Sum or Kruskal-Wallis tests. Differences were considered statistically significant when $p < 0.05$. Posthoc pairwise comparisons were performed using the Tukey-Kramer approach.

DATA AND CODE AVAILABILITY

Raw two-photon data imaging data have not been deposited in a publicly available repository due to file size, but all relevant data and code for this study can be made available by the Lead Contact Michael Brecht, michael.brecht@bccn-berlin.de upon reasonable request.